Switched control of a SCARA robot with shared actuation resources ⋆

A. van der Maas * **Y.F. Steinbuch** ** **A. Boverhof** *** **W.P.M.H. Heemels** *

* *Department of Mechanical Engineering, Control System Technology Group, Eindhoven University of Technology, 5600MB, Eindhoven, The Netherlands*
(e-mail: A.v.d.Maas@tue.nl, M.Heemels@tue.nl).
** *STORM Eindhoven, Eindhoven University of Technology, Horsten 8, 5612 AX, Eindhoven, The Netherlands*
(e-mail: Y.Steinbuch@storm-eindhoven.com)
*** *VDL Enabling Technologies Group B.V., Achtseweg Noord 5, 5651GG, Eindhoven, The Netherlands*
(e-mail: Adrie.Boverhof@vdletg.com)

Abstract: Increasing performance demands on industrial motion systems often lead to more expensive hardware components and thus a high bill of materials. Given this trend, it is of interest to find solutions that still can provide good performance, but can be used to reduce the overall bill of materials. In this paper, such a solution is proposed by sharing actuation resources between several actuators and using advanced motion control algorithms for the resulting switched system to meet the performance requirements. Obviously, by the sharing of resources, less hardware components are needed, thereby significantly lowering the bill of materials. We demonstrate this solution on an industrial SCARA robot, where it is proposed to use a single amplifier to serve several actuators, rather than a separate amplifier for each actuator. Based on a switched nonlinear model of the robot, switched PID-type controllers are explored that connect to the industrial control practice. The potential of the proposed approach is shown both in simulations and real experiments on an industrial SCARA robot.

Keywords: Control applications, switching systems, hybrid systems, robotics, motion control

1. INTRODUCTION

Robotic handling systems are important in industrial applications, with increasingly higher demands on the accuracy and throughput. Generally, more expensive hardware components are used to comply with the increased performance specifications. However, in several situations it might be of interest to use cheaper hardware solutions to decrease the overall bill of materials, while advanced motion control algorithms are exploited to meet the desired accuracy and throughput requirements. One example, being the benchmark case in this paper, is the control of a robotic system that has multiple actuators, each of them individually driven by its own dedicated motor/amplifier pair. To reduce the bill of materials it could be of interest to use only one (or a few) amplifiers that are shared by the different actuators, thereby reducing the number of amplifiers. It is clear that to achieve this reduction, non-standard motion control algorithms are required that determine the continuous input (voltage to the amplifier) and the switching signal (which actuator is allowed to use the shared resource) to still meet the performance requirements.

A SCARA [1] robotic system is used in this paper as a case study to investigate the feasibility and potential of amplifier sharing, however, the proposed methods can be applied in different application scenarios as well. SCARA robots are specifically useful for applications where the available space is limited, e.g., applications in vacuum, where the space should be kept as small as possible, such that the vacuum can be realized rapidly. A wide range of applications is available, such as solar cells production, LED manufacturing, wafer handling in lithographic machines, and many other systems in the semiconductor industry. The idea of amplifier sharing was already mentioned in Driessen et al. (2011) for single-stage planar actuators, with the focus on the required electronics behind amplifier sharing. The advanced control required to allow for this sharing was not considered in Driessen et al. (2011). Therefore, we investigate this control design problem in this paper.

The SCARA robot consists of an upper and a lower arm, and has three degrees of freedom associated with the rotation of the arms and translation along the z-axis. Currently three amplifiers are used to control the three actuators related to the degrees of freedom, which are the wrist, elbow and shoulder of the robot arm, see also Fig. 1 below. The possibility to remove a single amplifier would already result in a significant cost reduction. As such, in this case, the focus will be on one amplifier that will be shared between the upper and lower arm of the robot, i.e., only one arm receives power at any given time instant. As a result, next to the power level (continuous input), also the choice which actuator is being powered (discrete decision) has to be made. As the robot dynamics are intrinsically nonlinear, a co-design problem is obtained for a switched nonlinear system, see, e.g., Liberzon (2003). The problem is of a co-design nature, as both discrete inputs (the active mode) and continuous inputs (the power level) have to be selected.

⋆ This research is supported by the Dutch Technology Foundation STW, carries out as a part of the CHAMeleon project "Hybrid solutions for cost-aware high-performance motion control" (no. 13896).

[1] SCARA stands for Selective Compliance Articulated Robot Arm

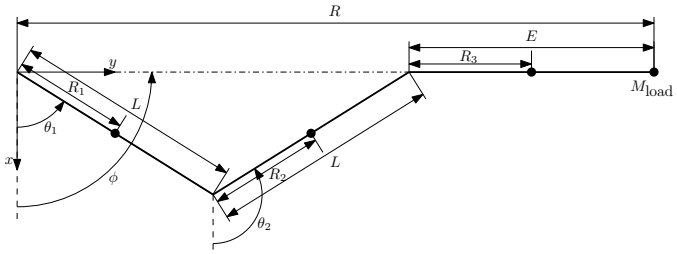

Fig. 1. Schematic top view of a SCARA robot. The two degrees of freedom θ_1 and θ_2 are included.

In this feasibility study, a controller design method is explored to solve the switched control problem by periodically switching power between both actuators combined with standard industrial controllers. In fact, based on periodically switching in which the switching frequency has to be determined, the currently available proportional-integral-derivative (PID) controllers for the upper and lower arms, designed for the case that each actuator has a dedicated amplifier, are retuned to account for the switching behavior. The PID controllers with and without switching are compared in simulations. In addition, experimental results are provided that show that satisfactory closed-loop behavior can indeed be achieved. These results underline the potential of reducing the bill of materials by sharing hardware components between multiple actuators and it serves as a proof of concept, encouraging further research in this interesting area.

In Sec. 2, the benchmark case is defined, focusing on the model of the system and the problem statement. In Sec. 3, the feedback controller design is discussed. In Sec. 4, simulation results are shown using the PID controller in a switching and non-switching configuration, based on a non-linear model of the robot. In Sec. 5, the simulations are experimentally validated on the industrial SCARA robot. In Sec. 6, the paper is concluded with an overview of the obtained results and recommendations for future research.

2. SCARA ROBOT PROBLEM FORMULATION

In this section, the SCARA robot, as shown in Fig. 1, is introduced in detail. In Sec. 2.1 a general description of the system is provided. In Sec. 2.2, a parameter-varying model of the SCARA robot is described. This model is used for the controller design, for which the requirements are given in Sec. 2.3. The section concludes with the problem statement for the switching controller design in Sec. 2.4.

2.1 System Description

The SCARA robot studied in this paper is generally used to place objects from a certain buffer into a process chamber. The SCARA robot is used as an object handler, the performance demands are high, leading to strict requirements on the controller of the robot. Since the object is typically not mounted physically to the wrist, the lateral forces have to be limited and collisions have to be avoided at all times.

The SCARA robot arm consists of three parts being an upper arm, a lower arm and a wrist, resulting in three degrees of freedom. The three degrees of freedom describe the orientations of the upper and lower arms, here, θ_1 and θ_2 are the absolute angles of the arms, respectively, as depicted in Fig. 1, and the

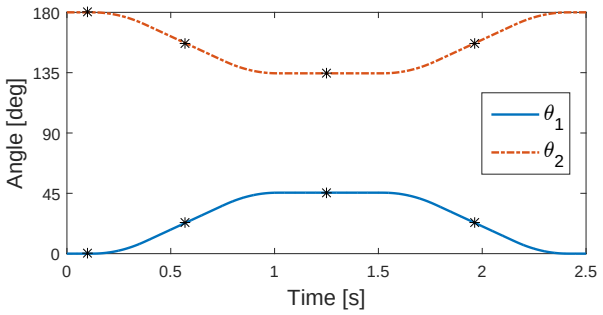

Fig. 2. Reference trajectories for extension (first second) and retraction (last second).

vertical position of the arm z. In the remainder of the paper, only the control of θ_1 and θ_2 will be considered. Each degree of freedom is (currently) actuated with an individual actuator/amplifier combination. The center of mass of the object (M_{load}) is positioned at the wrist of the SCARA robot, which is the main point of interest for the performance criterion. The wrist is, by design, always oriented in line with the center of the robot, and, as such, it is not considered as a degree of freedom. A typical motion of the system is shown in Fig. 2, which describes the extension and retraction of the arm.

The position of the object relative to the center of the robot can be expressed in polar coordinates. The radius of this position is described by

$$R = 2L\cos\left(\frac{\theta_1 - \theta_2}{2}\right) + E, \tag{1}$$

and the orientation by

$$\phi = \frac{\theta_1 + \theta_2}{2}, \tag{2}$$

as shown in Fig. 1. This results, in the Cartesian coordinate system, in

$$x_{\text{load}} = R\cos(\phi), \qquad y_{\text{load}} = R\sin(\phi), \tag{3}$$

indicating the position of the center of the load M_{load}.

2.2 Model description

A full nonlinear model of the SCARA robot has been derived based on first principle modeling with states

$$x = \begin{bmatrix} \theta_1 & \theta_2 & \theta_{m,1} & \theta_{m,2} & \dot{\theta}_1 & \dot{\theta}_2 & \dot{\theta}_{m,1} & \dot{\theta}_{m,2} \end{bmatrix}^\top, \tag{4}$$

where θ_1 and θ_2 represent the orientation of the upper and lower arm, respectively, as mentioned before. The states $\theta_{m,1}$ and $\theta_{m,2}$ are related to the rotations of the actuator axis corresponding to the two degrees of freedom. The states $\dot{\theta}$ represent the velocity of the respective angles. This results in the system dynamics described by

$$\dot{x} = f(x) + Bu + d \tag{5}$$

with $u = \begin{bmatrix} u_1 & u_2 \end{bmatrix}^\top$ the inputs of the system, i.e., the voltages V_1 and V_2 applied to the amplifiers, and d the disturbances, including friction, acting on the system. The matrix $B \in \mathbb{R}^{8\times 2}$ is given by $B = \begin{bmatrix} B_1 & B_2 \end{bmatrix}$, and $f : \mathbb{R}^{n_x} \mapsto \mathbb{R}^{n_y}$ a nonlinear function. For space reasons, the full nonlinear model is not included in this paper, but the non-parametric linearized model used for control is provided in Sec. 3.1.

2.3 Design requirements

The main control objective is to obtain reference tracking with minimal error, i.e., it would be desirable to have $x_{\text{load}} = x^*_{\text{load}}$ and $y_{\text{load}} = y^*_{\text{load}}$, where the superscript $*$ indicates the reference signal. The tracking performance can be divided into an error in the orientation of the robot, and an error in the reference tracking of the end-effector. Mathematically, these errors are given by

$$\epsilon_{\text{line}}(t) = \frac{y_{\text{load}}(t)x^*_{\text{load}}(t) - x_{\text{load}}(t)y^*_{\text{load}}(t)}{\sqrt{x^*_{\text{load}}(t)^2 y^*_{\text{load}}(t)^2}}, \tag{6}$$

$$\epsilon_{\text{abs}}(t) = \sqrt{\left(x^*_{\text{load}}(t) - x_{\text{load}}(t)\right)^2 + \left(y^*_{\text{load}}(t) - y_{\text{load}}(t)\right)^2}, \tag{7}$$

which specifically represent the deviations of the wrist orientation with respect to the central axis of the robot and the absolute tracking error, respectively. The specifications for the design of the controllers are given by

$$|\epsilon_{\text{line}}(t)| \leq 1 \text{ mm} \qquad \epsilon_{\text{abs}}(t) \leq 10\ \mu\text{m}, \tag{8}$$

where the absolute error specification does not need to hold for all $t \in \mathbb{R}_{\geq 0}$, but only when the SCARA robot is in the fully extended and retracted position. In these orientations of the robot, the positioning performance is most critical, since at these times, the objects are moved on and from the robot.

2.4 Resource Sharing Problem Statement

The aim of this paper is to obtain a control strategy to allow for resource sharing, specifically, sharing an amplifier between multiple actuators. In terms of the input, this corresponds to the constraint

$$u_1(t) = 0 \qquad \vee \qquad u_2(t) = 0 \quad \text{for all} \quad t \in \mathbb{R}_{\geq 0}. \tag{9}$$

This corresponds to only powering one actuator at a time, and therefore, (5) can be rewritten as the switched system

$$\dot{x} = \begin{cases} f(x) + B_1 u_1 + d, \\ f(x) + B_2 u_2 + d, \end{cases} \tag{10}$$

with u the supplied voltage to the amplifier and d a possible disturbance.

In the switched control situation, the system should meet the same requirements as listed in Sec. 2.3. In this paper, periodical switching is used, typically at a slower frequency than the sample frequency. Using slower switching frequencies relaxes the effects of switching on the electronics, since switching every sample can be hard to obtain physically. The use of aperiodic switching strategies is a topic in future research.

3. FEEDBACK CONTROLLER DESIGN

In this section, the linear feedback controller design is discussed. To enable tuning of a non-switching PID-type controller, a linear(ized) model is helpful. In Sec. 3.1, a nonparametric linear parameter-varying model is derived for various operating conditions. In Sec. 3.2, a non-switching PID controller is derived, which robustly stabilizes the four relevant operating conditions identified in Sec. 3.1. Finally, in Sec. 3.3, the control strategy for the switching controller is given.

3.1 LPV modeling

The focus is on using two actuators sharing one amplifier, thereby putting restrictions from (9) on the input u leading to a switched control system as in (10), of which the switching law will be defined periodically. To design the controller, it is of interest to obtain insight in the dynamics of the system, which will be done using nonparametric linear models of the system. A parametric linear model of the system could be obtained by linearizing the nonlinear model along the desired trajectory of the system, as depicted in Fig. 2, however, this is outside the scope of this paper.

For the design of the controller, which will be a (switched) PID-type of controller to ease the industrial implementability and acceptance in this case, a non-parametric model will be used. Since the system is heavily dependent on the orientation of the system, the model has to be based on several operating conditions, i.e., several values for θ_1 and θ_2. In this paper, various operating conditions are selected along the reference trajectory using frequency response functions (FRFs) of a linear parameter-varying (LPV) system, see, e.g., (Pintelon and Schoukens, 2012; van der Maas et al., 2016) for some examples of non-parametric identification of LPV systems. Note that the knowledge of the full nonlinear model is not used in the identification. The operating points under consideration are indicated in Fig. 2 by the stars, i.e., at retracted position, at full forward and backward velocity and at the extended position.

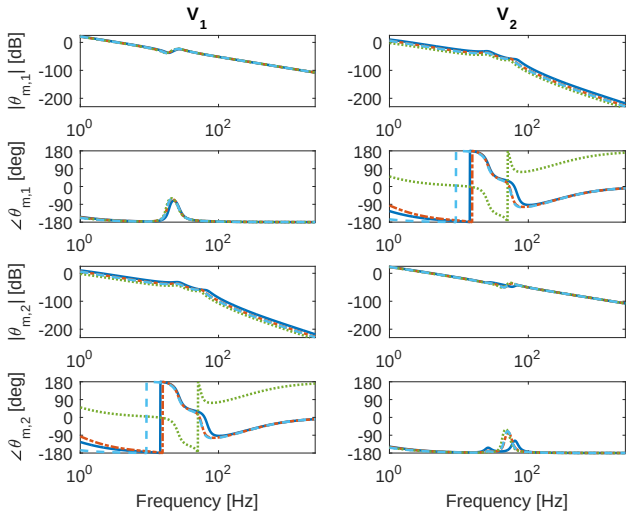

Fig. 3. FRFs of the four operating points (in different color-dash style combinations) of the MIMO system.

The multiple-input-multiple-output (MIMO) Bode plots are shown in Fig. 3, for the four operating points. The inputs of the system are the voltages $u_1 = V_1$ and $u_2 = V_2$ applied to the amplifiers, and the outputs as the motor angles $\theta_{m,1}$ and $\theta_{m,2}$, which are the measured states. It can be seen that the four operating points have rather similar dynamics. The main difference that can be observed is the 180 degrees phase shift in one of the positions compared to the other three, which can be related to a minus sign. Significant off-diagonal terms are present in the Bode diagrams, therefore, the design of the PID controller cannot be easily obtained using decoupled SISO designs. Since the dynamics at different operating points show similar behavior, it seems reasonable to approach the highly nonlinear model from (5) by the nonparametric LPV system.

3.2 PID design without switching

The controller design is based on the system without switching, described by the linear system in the four Bode plots of the MIMO system in Fig. 3. A single, robustly stabilizing controller is designed for the systems at the four operating points as discussed in Sec. 2.2. The stability of the closed-loop system in general cannot be guaranteed based on this design. However, local asymptotic stability around the reference trajectory is obtained, since the controller stabilizes each of the (closely correlated) operating points, see, e.g., Shamma (2012); Oliveira and Peres (2008); da Silva et al. (2008). The dynamics of the system are not decoupled, therefore, sequential loop closing methods are used to design the controller, see, e.g., (Steinbuch et al., 2010, Sec. 27.5.6) and (Maciejowski, 1989, Chapter 4).

A PID controller is designed that stabilizes the four operating points. In Fig. 4 the Bode diagram is shown for the open-loop transfer function $H_1(s) = C_1(s)P_{11}(s)$, which is stable with good robustness margins; a gain margin of 10.8 dB and a phase margin of 67 degrees, see e.g., Franklin et al. (2006) for a the definitions of these robustness margins. The bandwidth of the system is between 16-18.4 Hz for the four operating conditions, i.e., the frequency at which the open-loop system crosses the 0dB.

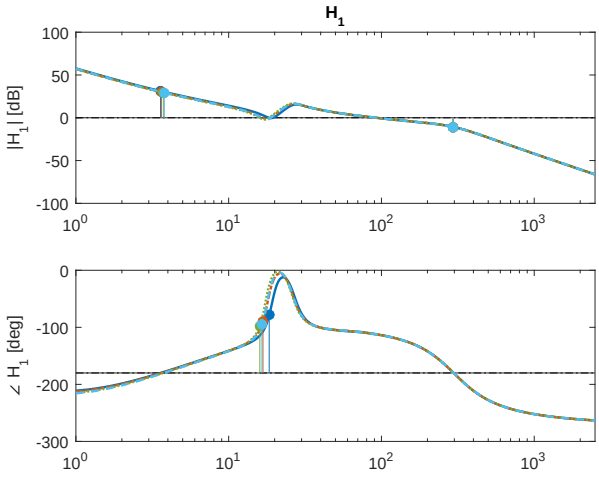

Fig. 4. Open-loop Bode diagram of H_1.

Fig. 5 shows the Bode diagram for the open-loop transfer function

$$H_2(s) = C_2(s)\left(P_{22}(s) - \frac{C_1(s)P_{12}(s)P_{21}(s)}{1 + C_1(s)P_{11}(s)}\right), \quad (11)$$

which is the final open-loop transfer function for the sequential loop shaping method. The system is again stable with good robustness margins; a gain margin of 14 dB and a phase margin of 65-67 degrees. The bandwidth of this open-loop system is between 27-29 Hz. Since the loop is closed using sequential loop closing, the stability of both H_1 and H_2 is sufficient to conclude stability of the full system in the individual operating points.

3.3 Switched Controller design

The PID controller as introduced in the previous section is used in the switching controller. It is chosen not to change the design of the controller, but simply amplify the controller by a factor

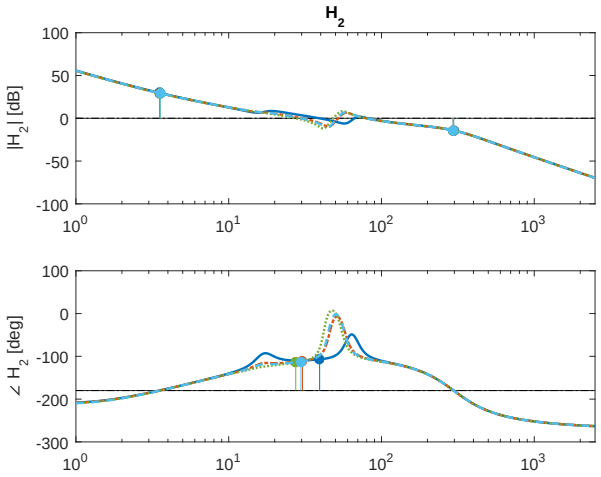

Fig. 5. Open-loop Bode diagram of H_2.

2, in order to obtain the same (average) effort to both actuators over the entire trajectory. Switching between the actuators is selected to be periodically, at a lower frequency than the sample frequency, such that the effects on the hardware are not too severe and the dynamical effects of switching in the electronics has a minimal effect. In a hybrid systems framework, see, e.g., Goebel et al. (2012), this switching controller can be written by flow dynamics $\mathcal{F}$ and jump dynamics $\mathcal{J}$

$$\mathcal{F} = \begin{cases} \dot{x} = f(x) + B_q u_q + d \\ \dot{q} = 0 \\ \dot{\tau} = 1 \end{cases}, \quad \mathcal{J} = \begin{cases} x^+ = x \\ q^+ = 3 - q \\ \tau^+ = 0 \end{cases} \quad (12)$$

where the system can stay in $\mathcal{F}$ as long as $\xi = \begin{bmatrix} x^\top & q & \tau \end{bmatrix}^\top \in \mathcal{C}$, with $\mathcal{C} = \{\xi \in \mathbb{R}^{n_x} \times \{1,2\} \times \mathbb{R}_{\geq 0} | \tau < T_{switch}\}$. The system has to make a jump in the dynamics when $\xi \in \mathcal{D}$, with $\mathcal{D} = \{\xi \in \mathbb{R}^{n_x} \times \{1,2\} \times \mathbb{R}_{\geq 0} | \tau \geq T_{switch}\}$. Note that, in this formulation, q indicates the active actuator, τ represents a timer to maintain the periodic switching, and T_{switch} the switching time.

No formal proof is given for the stability of this controller, further studies are required to guarantee this using Lyapunov types of stability criteria.

4. SIMULATION RESULTS

In this section, the PID controller is implemented in simulations on the system, both with and without switching (actuator sharing). Throughout the simulations and experimental validations, the reference trajectory from Fig. 2 is used. As explained in Sec. 2.4, switching occurs periodically at a certain switching frequency (typically lower than the sampling frequency). The switching implies that only one of the two actuators is served by the actuator at all times, as indicated in (9).

First, a simulation is shown using the PID controller designed in Sec. 3.2, without switching. The results of this simulation is shown in Fig. 6 in blue in terms of the line error. The line error for the non-switching simulation is maximally 0.25mm, which is well within the 1mm specification. In the region where performance is crucial, i.e., in the fully extended and retracted position at $t \in [1, 1.4]$s and $t \in [2.4, 2.8]$s, the error is within the 10μm band, indicated by the black box.

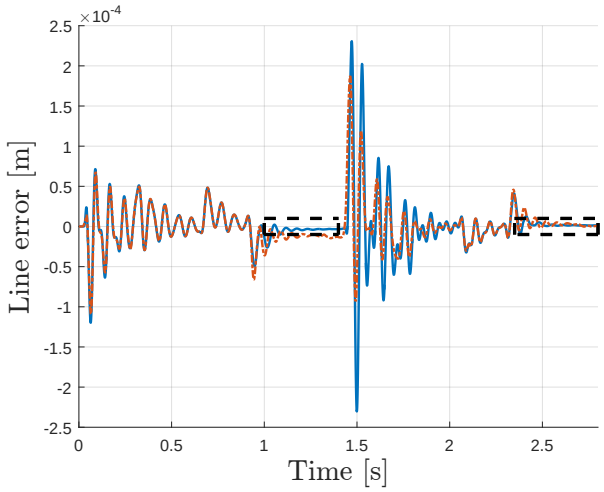

Fig. 6. Line error ϵ_{line} with (red-dash-dotted) and without (blue) switching.

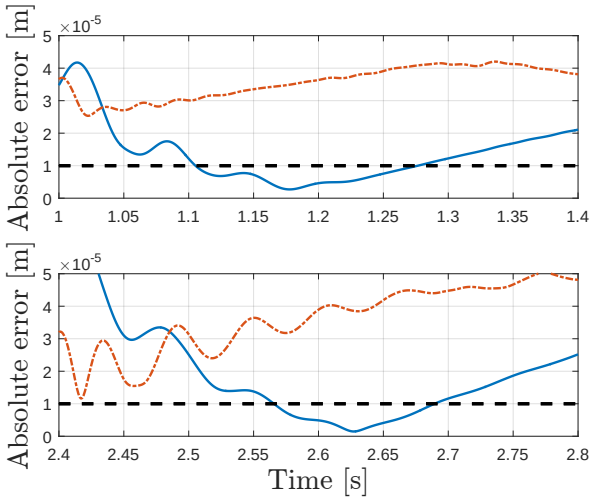

Fig. 7. Absolute error ϵ_{abs} with (red-dash-dotted) and without (blue) switching.

In Fig. 6, the line error of the system with switching controllers is shown as well, with a switch occurring every 1 ms (so a 1 kHz switching frequency), in the red dash-dotted line. The performance for both controllers is comparable. Overall, the switching controller has a slightly smaller line error, which is clearly visible between 1.4 and 2 seconds. However, in the fully extended position, the non-switching controller has a better performance. It can be seen that the switching controller has a small constant offset compared to the non-switching controller.

The corresponding absolute errors of the simulations are shown in blue in Fig. 7. It can be seen that for the non-switched controller, the specified accuracy is reached, however, not in the full period of extension or retraction. The absolute error for the switched controller, as shown in red, shows a decreased performance. Overall, the performance for both controllers is comparable, which provides sufficient confidence in the switching controller to reduce the number of actuators.

The main goal of this paper is to show the potential of the switching controller, i.e., using amplifier sharing. Therefore, the performance specifications on the line and absolute errors are not the main focus. However, it has been shown that, by including feedforward to this system, the performance specification are met.

Different switching rates have been implemented in simulations, i.e., switching at 500Hz, 250Hz and 100Hz, which showed that an optimum for the performance of this system is achieved when switching at 250Hz, since this is the lowest frequency that does not result in oscillations due to the switching, and does not deteriorate the performance compared to the non-switched system.

5. EXPERIMENTAL RESULTS

In this section, the performance of the proposed approach is validated using experiments on an industrial SCARA robot, as shown in Fig. 8.

Fig. 8. Experimental SCARA robot. The object is normally positioned at the end of the wrist, with its center between the two black rubber rings.

Three encoders are present on the system, measuring the actuator angles collocated, i.e., directly measuring the actuated states z, $\theta_{\text{m},1}$, and $\theta_{\text{m},2}$. The encoder resolution is 1.5mrad for the rotational encoders, with a gear ratio of 1/50 to the actual motions, resulting in a resolution of 0.03mrad. This resolution results in a sparse grid for the absolute error, where a single encoder pulse results in a jump from 10μm to 18μm, therefore, except for perfect tracking, i.e., $\epsilon_{\text{abs}} = 2\mu$m, the specification cannot be verified in practice. Rather than checking the specifications, only comparisons are made in this section between the controllers with and without switching. All experiments in this section have been performed 10 times to achieve some reliable results. Actual switching of a single amplifier between the two actuators is not yet available. Therefore, in this exploratory study, the switching is emulated in software enforcing (9).

In Fig. 9, the resulting line errors for experiments with and without actuator switching are shown. It can be seen that the experimental performance is, as expected from simulations, comparable. For completeness, also the absolute errors are included in Fig. 10, which show a constant value for each of the controllers. Again, as expected, the switching controller has a slightly larger absolute error than the non-switching controller.

Since the actual specifications on the absolute error do not give enough information due to limited sensor resolution, the 2-norm of the errors in the time windows [1,1.4] and [2.4,2.8], i.e., the fully extended and retracted positions, over the 10 experiments are compared. In Table 1, these 2-norms are summarized for both controllers. It can be seen that the line error

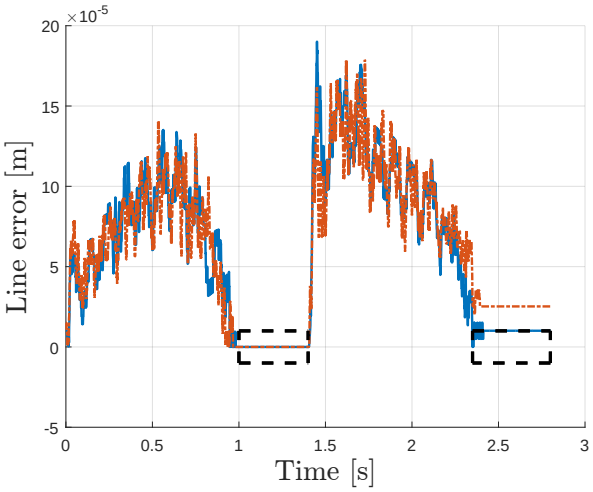

Fig. 9. Line error ϵ_{line} from experiments with (red-dash-dotted) and without (blue) switching.

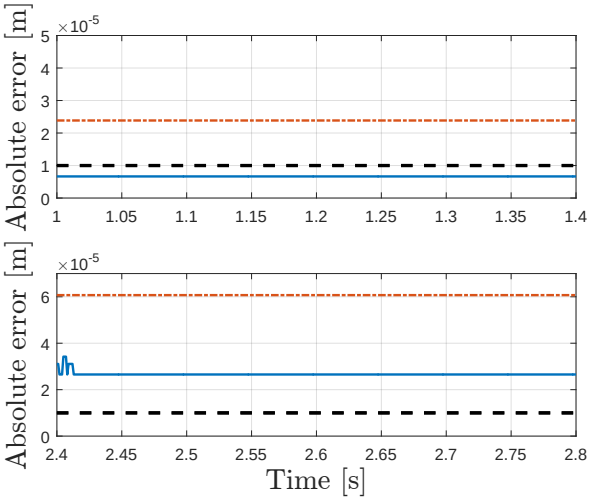

Fig. 10. Absolute error ϵ_{line} from experiments with (red-dash-dotted) and without (blue) switching.

Table 1
Comparison of 2-norm of the line and absolute errors in the fully extended and retracted orientation.

Switching	ϵ_{line} [m]	ϵ_{abs} [m]
Without	$3.22 \cdot 10^{-3}$	$3.19 \cdot 10^{-4}$
With	$3.20 \cdot 10^{-3}$	$3.78 \cdot 10^{-4}$

reduces slightly when switching is introduced, however, the absolute error has increased.

Using these experiments, that show comparable results between the switching and non-switching controllers, the potential of the switching controller setup has been shown.

6. CONCLUSION

In this paper, an exploratory study has been presented to investigate the potential of sharing hardware recourses, in this case amplifiers of the actuators, for robotic systems to lower the bill of materials. To comply with the performance specifications, advanced motion control tools are required for the resulting switched system. The potential and feasibility of resource sharing has been shown on a SCARA robot arm.

A MIMO controller has been designed based on PID controllers using sequential loop shaping. This controller has been implemented in simulations for both the switched and non-switched controllers, showing comparable results. Since the switching controller does not result in a significantly decreased performance in simulations or experiments, the method appears to be a feasible option to reduce the bill of materials in industrial practice.

So far, the switching has been implemented periodically, i.e., switching at a certain rate. In future work, more advanced, optimal controllers might be used, not only to optimize the input signal, but also the switching sequence, thereby increasing the performance even more. Optimizing the switching sequence might lower the switching frequencies, thereby reducing the strain on the power electronics that also need to be designed.

REFERENCES

da Silva, M.M., Desmet, W., and Van Brussel, H. (2008). Design of Mechatronic Systems With Configuration-Dependent Dynamics : Simulation and Optimization. *Transactions on Mechatronics*, 13(6), 638–646.

Driessen, A., Wijnands, C., Duarte, J., and Roes, M. (2011). Reduction of the number of power amplifiers for an advanced single-stage planar actuator. In *Proceedings of the 14th European Conference on Power Electronics and Applications and Exhibition*, 1–10. Birmingham, UK, England.

Franklin, G.F., Powell, J.D., and Emami-Naeini, A. (2006). *Feedback Control of Dynamic Systems*. Pearson Education, Inc., Upper Saddle River, New Jersey, USA, 5 edition.

Goebel, R., Sanfelice, R.G., and Teel, A.R. (2012). *Hybrid Dynamical Systems, Modeling, Stability and Robustness*. Princeton University Press, 41 William Street, Princeton, New Jersey, USA, 1 edition.

Liberzon, D. (2003). *Switching in Systems and Control*. Systems & Control: Foundations & Applications. Springer Science + Business Media, LLC, New York, USA.

Maciejowski, J. (1989). *Multivariable Feedback Design*. Addison-Wesley Publishing Company.

Oliveira, R.C.L.F. and Peres, P.L.D. (2008). Robust stability analysis and control design for time-varying discrete-time polytopic systems with bounded parameter variation. In *Proceedings of the American Control Conference*, volume 1, 3094–3099.

Pintelon, R. and Schoukens, J. (2012). *System Identification*. John Wiley & Sons.

Shamma, J.S. (2012). An Overview of LPV Systems. In J. Mohammadpour and C.W. Scherer (eds.), *Control of Linear Parameter Varying Systems with Applications*, chapter 1, 3–26. Springer US.

Steinbuch, M., Merry, R.J.E., Boerlage, M.L.G., Ronde, M.J.C., and Molengraft, M.J.G.V.D. (2010). Advanced Motion Control Design. In *Control System Applications*, chapter 27.

van der Maas, A., van der Maas, R., Voorhoeve, R., and Oomen, T. (2016). Frequency Response Function Identification of LPV Systems : A 2D-LRM Approach with Application to a Medical X-ray System. In *Proceedings of the American Control Conference*, 4598–4603. Boston, MA, USA.